Force transduction and strain dynamics in actin stress fibres in response to nanonewton forces

Louise Guolla[1], Martin Bertrand[1], Kristina Haase[1] and Andrew E. Pelling[1,2,*]

[1]Department of Physics, MacDonald Hall, 150 Louis Pasteur, University of Ottawa, Ottawa, ON, K1N 6N5, Canada
[2]Department of Biology, Gendron Hall, 30 Marie Curie, University of Ottawa, Ottawa, ON, K1N 6N5, Canada
*Author for correspondence (a@pellinglab.net)

Accepted 20 September 2011
Journal of Cell Science 125, 603–613

doi: 10.1242/jcs.088302

Summary

It is becoming clear that mechanical stimuli are crucial factors in regulating the biology of the cell, but the short-term structural response of a cell to mechanical forces remains relatively poorly understood. We mechanically stimulated cells transiently expressing actin–EGFP with controlled forces (0–20 nN) in order to investigate the structural response of the cell. Two clear force-dependent responses were observed: a short-term (seconds) local deformation of actin stress fibres and a long-term (minutes) force-induced remodelling of stress fibres at cell edges, far from the point of contact. By photobleaching markers along stress fibres we were also able to quantify strain dynamics occurring along the fibres throughout the cell. The results reveal that the cell exhibits complex heterogeneous negative and positive strain fluctuations along stress fibres in resting cells that indicate localized contraction and stretch dynamics. The application of mechanical force results in the activation of myosin contractile activity reflected in an ~50% increase in strain fluctuations. This approach has allowed us to directly observe the activation of myosin in response to mechanical force and the effects of cytoskeletal crosslinking on local deformation and strain dynamics. The results demonstrate that force application does not result in simplistic isotropic deformation of the cytoarchitecture, but rather a complex and localized response that is highly dependent on an intact microtubule network. Direct visualization of force-propagation and stress fibre strain dynamics have revealed several crucial phenomena that take place and ultimately govern the downstream response of a cell to a mechanical stimulus.

Key words: Actin, Atomic force microscopy, Cell mechanics, Cytoskeleton, Mechanotransduction, Strain

Introduction

Mechanotransduction, the transmission of a mechanical stimulus into a useful chemical or biochemical signal, is a concept being rigorously studied in the field of biophysics (Jaalouk and Lammerding, 2009; Wang et al., 2009). It is known that the surrounding mechanical environment of a cell, and the environment itself, play an important role in determining stem cell fate, apoptotic and mitotic progression, gene regulation and in disease processes such as cancer metastasis (Chiquet et al., 2007; Chowdhury et al., 2010; Engler et al., 2006; Hogan et al., 2009; Kunda et al., 2008; Lopez et al., 2008; Pelling et al., 2009; Maloney et al., 2010). There is increasing evidence that one major key to understanding mechanotransduction lies within the dynamics of the cytoskeleton response to mechanical stimuli (Fletcher and Mullins, 2009). In particular, actin stress fibres (SFs) have been implicated as a having a major role in these processes by transmitting and generating nanomechanical forces. In the 1980s, experiments were performed wherein protruded extensions of fibroblast cells retracted following detachment from the surface by glass needles (Albrecht-Buehler, 1987). It was concluded that this retraction must be due to either the movement or depolymerisation of actin filaments, as neither a drug inhibiting the re-polymerization of actin nor a drug inhibiting microtubule (MT) polymerization had any effect on the observed retraction. Similarly, early micropipette aspiration experiments determined that after the application of a shear stress, unlike cells that had not experienced a mechanical stimulus, epithelial cells had stiffer mechanical properties and retained their elongated shape (as seen by staining for actin filaments) following detachment from the culture surface (Sato et al., 1987).

Laser ablation experiments, in which actin SFs are severed using femtosecond pulses, suggest that these earlier observed trends are largely due to mechanical tension along the SF (Kumar et al., 2006). Retracting SFs also appear to form pseudo focal adhesion (FA) sites along the basal membrane as they slide along it (Colombelli et al., 2009). Zyxin, an FA protein, has been shown to act as a mechanical ‘tension sensor’. Zyxin appears to localize at points of increased tension along the actin cytoskeleton and at adhesion sites, both new and old, and disappears immediately following a loss of tension (Colombelli et al., 2009; Nix et al., 2001; Rottner et al., 2001). As FAs directly link the cytoskeleton to the extracellular environment, many investigations have been carried out on them (Burridge et al., 1988; Mierke, 2009; Weisberg et al., 1997). Early investigations have shown that the cytoskeleton can deform in response to applied forces. Actin SFs and MTs have been shown to deform in response to large-scale indentation with micropipettes. When microbeads or microneedles are bound to the cell surface and pulled, the applied force is propagated through the cytoskeleton to the nucleus, resulting in considerable global deformation (Maniotis et al., 1997). Indentation of cells with 10 μm beads has revealed how actin can transmit and focus applied forces to activate mechanosensitive ion channels (Hayakawa et al., 2008). When

Journal of Cell Science

endothelial cells experience a fluid flow the cytoskeleton undergoes shear-stress-induced deformation that results in FA remodelling and allows for the quantification of internal strain dynamics (Mott and Helmke, 2007; Ueki et al., 2010). By contrast, locally applied forces to cell membranes can result in calcium ion flux (Charras and Horton, 2002a; Charras et al., 2004; Formigli et al., 2007a; Ko and McCulloch, 2000) and localized, yet highly heterogeneous, force propagation and deformation of the cytoarchitecture that is mediated by the cytoskeleton as a whole (Hu et al., 2004; Silberberg et al., 2008).

Atomic force microscopy (AFM) (Binnig et al., 1986) has emerged as a major tool for investigating mechanical signalling pathways within cells (Costa et al., 2006; Czajkowsky et al., 2000; Haupt et al., 2006; Lehenkari et al., 2000; Radmacher, 2007; Trache and Lim, 2009). Originally intended for use as a topographical tool (Binnig et al., 1986), the ability of AFM to apply known controlled forces to living cells was quickly applied in the field of cell biology (Radmacher et al., 1992). By the 1990s, AFM was being used to confirm and expand upon rheological measurements on cells (Henderson et al., 1992; Hoh and Schoenenberger, 1994; Radmacher et al., 1992). Fluorescent dyes, particularly fluorescent proteins has become extremely useful for direct visualization of the effect of applied force on the inner structure of the cell (Heidemann et al., 1999). The combination of AFM with simultaneous fluorescence and laser scanning confocal microscopy (LSCM) has allowed direct correlation of local mechanical properties measured with AFM to specific subcellular structures (Lehenkari et al., 2000; Pelling et al., 2009; Silberberg et al., 2008) and the cytoskeleton (Charras and Horton, 2002a; Costa, 2006; Ko and McCulloch, 2000; Pelling et al., 2007a; Pelling et al., 2009; Rotsch and Radmacher, 2000). However, the relative influences of the three major filaments systems (actin SFs, MTs and intermediate filaments) on the mechanical properties of the cell are also dependent on physiological state (Kunda et al., 2008; Matzke et al., 2001; Pelling et al., 2009; Maloney et al., 2010). In a previous study (Trache and Lim, 2009), measurements of force-induced SF reorganization were taken over the course of 80 minutes with ~8- to 14-minute time resolution. The application of mechanical force resulted in the reorganization of SFs, although no detailed analysis of the magnitude of the applied force, deformation or strain profiles were performed.

Although the long-term (hours to days) downstream effects of physical forces on cell behaviour are being intensively studied, it is clear that one of the most immediate (seconds to minutes) responses of a cell to force is structural deformation, which occurs well before structural remodelling and changes in gene expression. However, the short-term structural response of a cell to a mechanical stimulus remains relatively poorly understood even though it influences long-term cell fate. In this study, we employed simultaneous AFM and high speed LSCM to apply locally controlled forces to the surface of living fibroblast cells that were expressing actin–EGFP over short time scales. By tracking the nanoscale movement of actin SFs over time in cells subjected to a range of forces (0, 1, 5, 10 and 20 nN), we demonstrated that locally applied forces do not result in large-scale isotropic deformation of the SF cytoskeleton. Rather, a small population of SFs undergo localized deformation or retraction. Of the SFs that move, two distinct types of behaviour are apparent. Within 20 seconds of force application, some SFs near to the point of contact (5–10 μm) move between 100 and 300 nm in a manner dependent on the applied force. SFs far from the point of contact (~30–50 μm) begin to deform at later times and continue to deform over the course of several minutes under a constant applied force. In response to mechanical loading, not only do SFs deform, but they experience relaxation and remodelling as a result of FA movement, which was visualized in cells expressing actin–EGFP and zyxin–mRFP. Experiments were also performed in which cells were pre-treated with nocodazole [a drug that specifically disrupts the MT network but not the actin cytoskeleton (Charras and Horton, 2002b; Pelling et al., 2009)] and Y27632, a rho kinase (ROCK) inhibitor [which inhibits the formation of actin SFs (Narumiya et al., 2000)]. The treatment with nocodazole reveals that MTs are required for the transmission of force resulting in SF deformation. In addition, treatment with Y27632 reveals that, in the absence of intact SFs, the cell deforms isotropically around the nucleus.

Finally, by photobleaching a regular array of spots along actin SFs we have been able to directly visualize the baseline and force-induced strain dynamics that take place along these structures. SFs experience highly heterogeneous negative and positive strain dynamics along their length. In a previous study (Peterson et al., 2004), whole cell contraction was induced with the serine/threonine phosphatase inhibitor calyculin A. It was reported that central SFs experience a positive strain (stretching), whereas peripheral regions experience a negative strain (contraction) in response to a drug-induced increase myosin activity. In the study reported here we examined basal SF strain dynamics and their response to a locally applied nanomechanical force. We observed a heterogeneous distribution of positive and negative strains every few microns along SFs instead of isotropic contraction–stretching in large regions of the SFs (Peterson et al., 2004). Moreover, the only observed difference in strain dynamics in response to a local force was an ~50% increase in strain fluctuations over time, which we attribute to increased myosin-II activity. This study reveals that the structural response of actin SFs in living fibroblast cells to controlled mechanical forces results in time-dependent deformation, heterogeneous actomyosin-induced strain dynamics, and absolutely requires the integration of several elements of the cytoarchitecture.

Results

Nanoscale movement of F-actin in response to a local force

AFM and LSCM were performed simultaneously on NIH3T3 cells transiently expressing actin–EGFP (Fig. 1A). The majority of SFs in our cells tended to form along the bottom of the cell, under the nucleus and parallel to the substrate (Fig. 1B). Movement was quantified by tracking multiple points along each SF in the cell as a function of time (Fig. 1C). Points along the SFs were spaced ~5 μm apart, which is below the persistence length of F-actin (Arai et al., 1999; Brangwynne et al., 2007; van Mameren et al., 2009). If an SF moved or deformed, a displacement vector was mapped from one of the initial tracking points to a new point on the fibre at the next time step, normal to the initial SF position (Fig. 1C). This method allowed us to quantify lateral displacements of the SFs relative to their initial position. However, this methodology precluded us from tracking SF stretching or contraction (strain dynamics) that did not result in lateral movement relative to the initial filament position. In all cases, the AFM tip was positioned over the centre of the nucleus. On average, the centre of the nucleus was within a

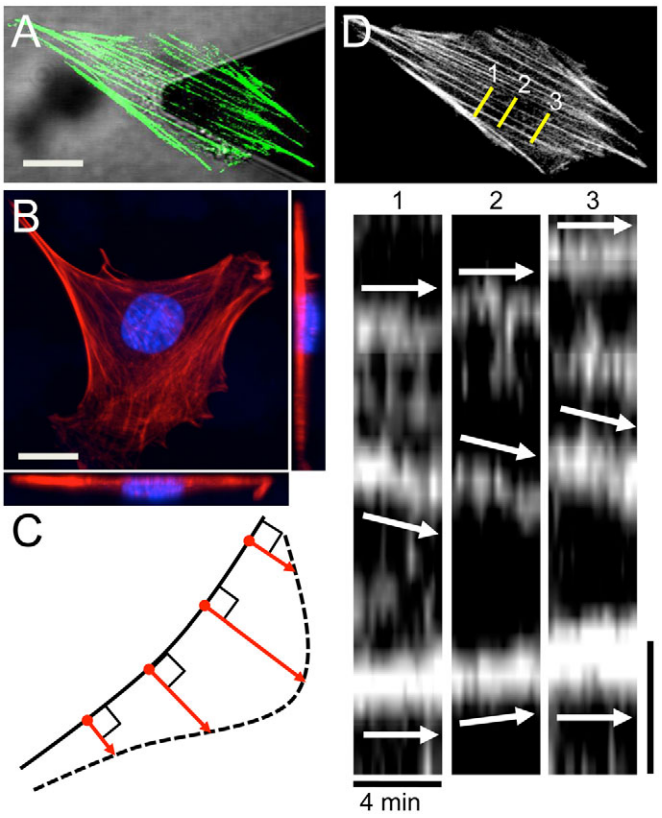

Fig. 1. SF localization, deformation and the tracked response to local forces. (**A**) An NIH3T3 cell expressing actin–EGFP under the AFM tip, which is centred over the nucleus. (**B**) A fixed cell stained for actin (red) and DNA (blue) reveals that F-actin tends to localize underneath the nucleus and parallel to the substrate as can be seen in the ZX and ZY projections (below and to the right). (**C**) SF tracking was achieved by mapping perpendicular displacement vectors (red) from an initial point on the filament at time zero (solid line) to a new point on the same filament at the next time step (dashed line) normal to initial filament position. (**D**) Kymographs reveal that not all SFs deform or move in response to force. In this case, kymographs were produced in three positions (numbered) perpendicular to three SFs. The middle SF deforms over time (downward arrow) but the two surrounding SFs do not deform to any extent (horizontal arrows). Scale bars: 15 μm (A,D); 15 μm (B); 2 μm (vertical bar D).

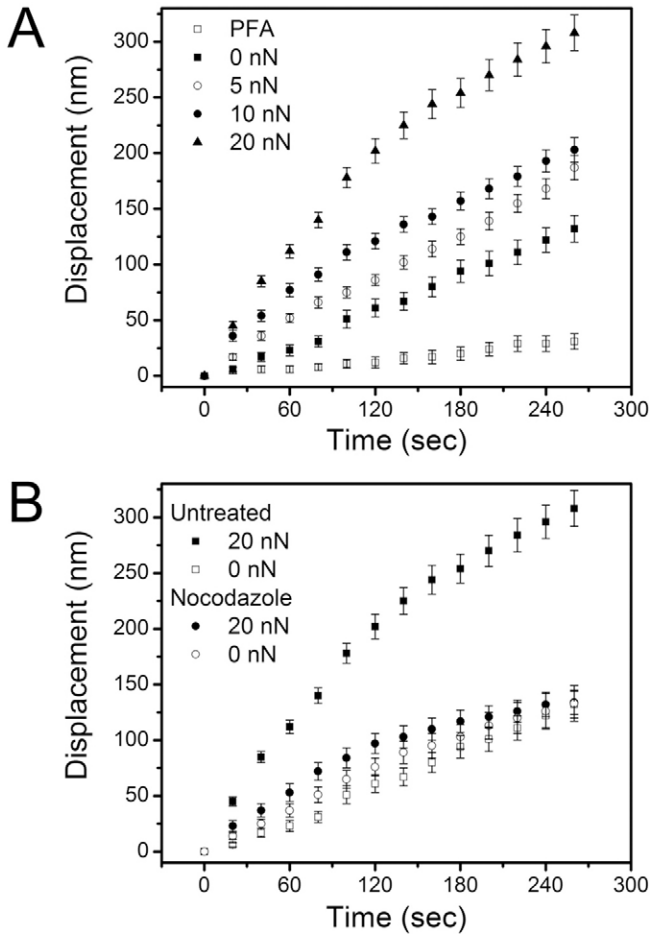

Fig. 2. Average displacement of SFs for all cells examined over time in response to locally applied forces. (**A**) The amount of SF movement is proportional to the applied force and occurs within 20 seconds. Displacement occurring in cells exposed to 0 nN force represents normal remodelling dynamics of SFs. A further control was performed on cells fixed with paraformaldehyde. Any displacement in this control can be attributed to microscope drift or error within the tracking method. (**B**) In some experiments cells were pre-treated with 10 μM nocodazole and either left unstimulated or exposed to a 20 nN force. The data for a cell experiencing a 0 or 20 nN applied force, without treatment with nocodazole, is re-plotted from A (squares). Following treatment with nocodazole, cells experiencing a 20 nN force only exhibited a minor increase in displacement compared with cells experiencing no force (with or without nocodazole pre-treatment; circles). This indicates the importance of an intact microtubule cytoskeleton for the transmission of force. All values are means ± s.e.m., $n=10$ cells for 5–20 nN, $n=5$ cells for 0 nN, $n=3$ cells for the PFA control, $n=4$ for nocodazole-treated cells at 20 nN.

radius of 4.4±1.6 μm from the cell centroid (supplementary material Fig. S1). Given that the typical diameter of a nucleus was 10–15 μm, the indentation point could be approximated as the centre of the cell. Kymographs were produced to examine the lateral displacement of SFs (Fig. 1D). On average, the amount of SF movement was proportional to the amount of force applied and occurred within 20 seconds of force application. A plot of the average total displacement on all filaments at each time point (Fig. 2) revealed that a force-dependent displacement of SFs was apparent after 20 seconds of force application and that this displacement increased over time for all forces (Fig. 2A). Control cells that were not exposed to any force also displayed SF displacements due to natural remodelling dynamics. Another control was employed in which cells were fixed with paraformaldehyde to examine any affects of microscope drift and tracking errors. However, it should be noted that in any given cell there were always SFs that did not display any visible movement (Fig. 1D). Displacement heat maps reveal that the spatial distribution of SF movement was not isotropic (Fig. 3). In other words, the cell and SFs did not simply bulge out in a circular deformation profile around the tip contact point. There was also no dependence of SF displacement magnitude with the distance from the tip contact point. In fact, SF displacements were localized and tended to evolve with time, and the fibres that did move exhibited one of two types of displacement: a slight lateral bulge in direct response to the AFM cantilever, generally within 5–10 μm of the tip location, or retraction at cell edges

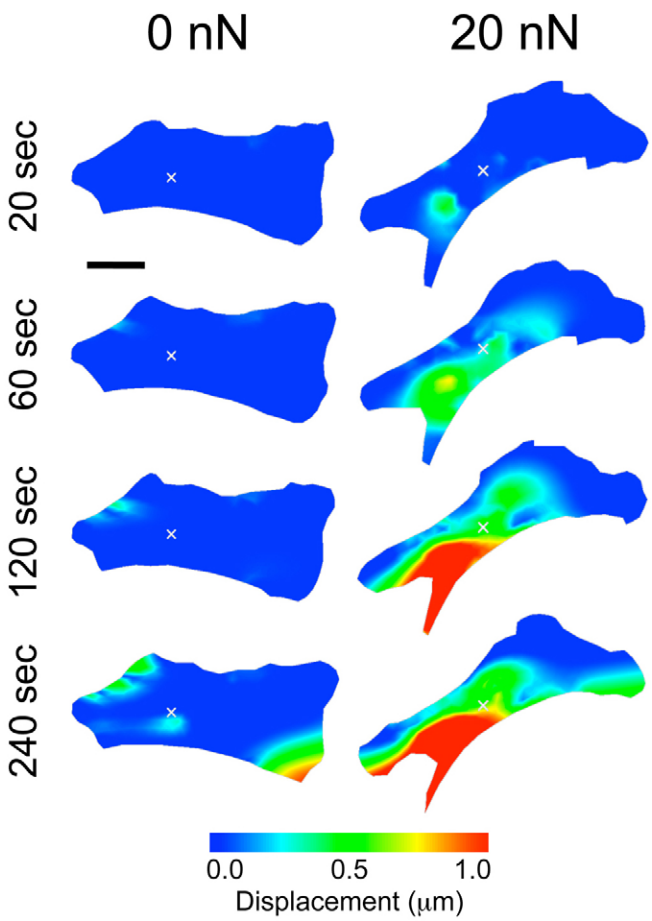

Fig. 3. Spatial heat maps of SF displacement in representative NIH3T3 cells experiencing 0 nN or 20 nN of applied force. The magnitude of the displacement vectors were plotted as spatial heat maps. It is clear that far more displacement occurs in response to 20 nN than to 0 nN. Displacement of SFs generally takes place immediately (within 20 seconds) and near to the point of force application (the contact point of the AFM cantilever is marked with a white 'x' and is over the centre of the nucleus). At later times retraction sometimes takes place at distant cell edges (red areas at 120 and 240 seconds after the application of 20 nN). Scale bar: 15 μm.

distant from the AFM cantilever (shown in the displacement maps in Fig. 3). Displacements taking place near the point of contact were a direct physical response to force and occurred within the first 60 seconds of force application. However, retraction dynamics at distant cell edges generally occurred much later (60–240 seconds) after force application, which suggests that the mechanical stimulus also results in biochemical remodelling of the SFs. These later retraction dynamics are responsible for what appears to be a continuously increasing average displacement at later time points (Fig. 2A).

To further investigate the force-stimulated SF displacement at cell edges, we generated cells transiently expressing actin–EGFP and zyxin–mRFP. Doubly transfected cells allowed us to examine the remodelling and/or movement FA sites that were mechanically and biochemically linked to SFs. After force application, it was observed that FA sites did not move if the SFs remained stationary or simply deformed (supplementary material Fig. S2). However, if the displacement of the SF was large then there was a correlated movement of FA sites. As can be seen in the kymographs (supplementary material Fig. S2), the FAs associated with non-moving SFs remained stationary and those associated with moving SFs appeared to slide along the surface with the actin. Moreover, none of the FA sites disappeared or diminished in intensity over the course of the measurement.

Effect of anti-cytoskeletal drugs on nanoscale F-actin movement

To determine the dependence of the observed SF displacement on various components of the cytoskeleton, we repeated the experiment on cells exposed to specific cytoskeletal inhibitors at the force resulting in maximal SF displacement (20 nN). Cells were pre-treated with 10 μM nocodazole (inhibits MT polymerization) or 10 μM Y27632 [a ROCK inhibitor, which prevents actomyosin contractility and SF formation (Fukata et al., 2001; Narumiya et al., 2000)]. These treatments had substantial effects on cytoskeleton morphology and cell cortical elasticity (Young's modulus, E), consistent with previous studies (Pelling et al., 2007b). It can be seen (supplementary material Fig. S3) that the cortical E of cells treated with nocodazole or Y27632 are significantly ($P<0.00001$) lower than cells with no drug treatment; however, nocodazole-treated cells had an intact SF cytoskeleton. Following treatment with nocodazole, an application of a 20 nN force had a much smaller effect on SF deformation, which was comparable with that of control cells not subjected to any force, with and without nocodazole treatment (Fig. 2B). However, the small displacement that did occur was apparent within 20 seconds following force application, as in the previous case. To visually demonstrate this difference, SF displacement heat maps were generated for nocodazole-treated cells at both 0 nN and 20 nN (Fig. 4). Cells treated with nocodazole showed no qualitative visual difference (compared with untreated cells) when exposed to 20 nN force. However, remodelling dynamics continued to occur at cell edges at later times.

To confirm that the depth of the indentation made by the AFM tip on nocodazole-treated cells and non-treated cells, as well as the cell heights were comparable, experiments were performed on cells transiently expressing the pleckstrin homology (PH) domain of phospholipase C (PLC)δ conjugated to EGFP (PH-PLCδ–EGFP). This protein is localized to the cell membrane (Hemsley et al., 2011), and thus provides a direct visualization of AFM tip indentation. As can be seen in Fig. 5 there was no significant difference between the heights of non-treated and treated cells, both before and after indentation (Fig. 5E). Although nocodazole did result in changes in the local cortical elasticity of the cell membrane, cells retained intact actin SFs, preventing an increase in cell height. Cross-sectional views of the cells undergoing AFM indentation (Fig. 5B,D) demonstrate that the indentation of the AFM tip was similar in non-treated and treated cells (~6–7 μm between the bottom of the cell and the tip apex). The tips did not penetrate through the entire cell and impact the surface of the dish, even after 4 minutes under a 20 nN force with or without nocodazole.

Y27632 treatment completely inhibited the formation of actin SFs, therefore the tracking method used previously was no longer valid. It can be observed that the application of a 20 nN force following treatment with 10 μM Y27632 immediately caused an isotropic 'bulge' in the cell surrounding the nucleus

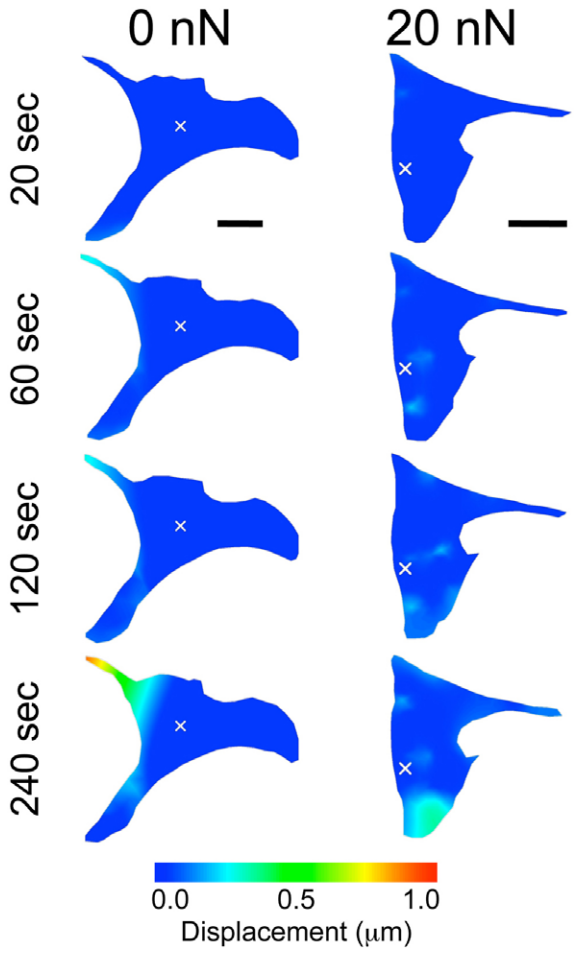

Fig. 4. Spatial heat maps of SF displacement over time in representative NIH3T3 cells experiencing 0 nN or 20 nN of applied force after treatment with 10 μM nocodazole. Spatial heat maps were constructed by plotting the magnitude of displacement vectors over time. It is clear that the SF displacements that occur in response to 20 nN without drug treatment is largely eliminated following treatment with nocodazole, as the heat map for 20 nN strongly resembles that for 0 nN. As before, the displacement that does occur is apparent as both a slight response near to the point of force (the contact point of the AFM cantilever is marked with a white 'x' and is over the centre of the nucleus) and as a retraction along the edges of the cell. Moreover, although the cells have a lower cortical elasticity after nocodazole treatment (supplementary material Fig. S3) no isotropic deformation is observed near the point of contact. Note that the displacement colour scale is identical to that in Fig. 3. Scale bars: 25 μm (0 nN); 15 μm (20 nN).

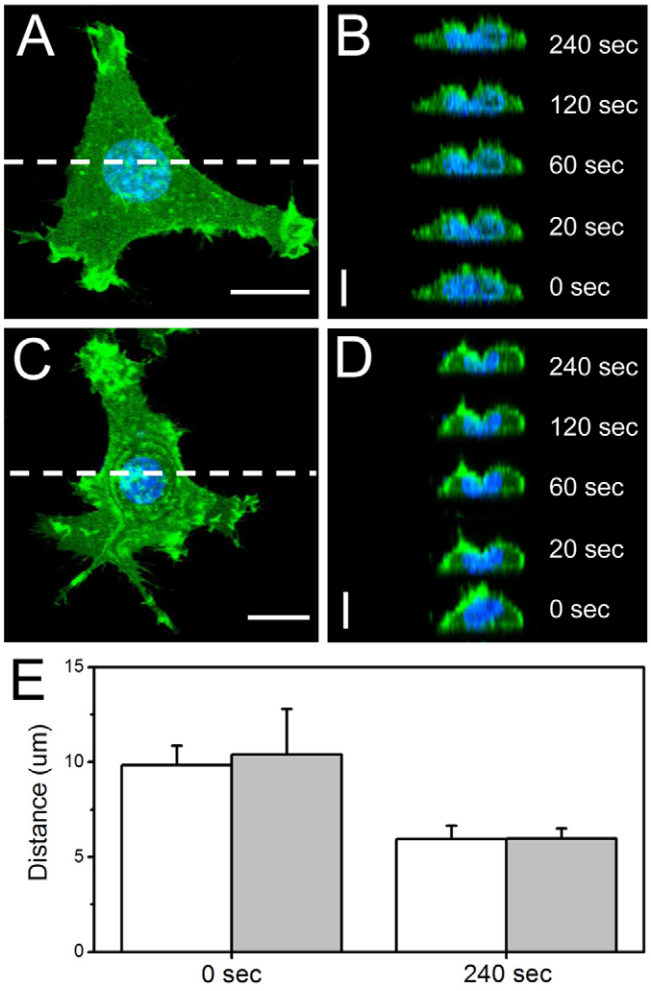

Fig. 5. Membrane deformation and AFM tip indentation. In order to compare the amount of indentation that occurs during force application in untreated (**A**,**B**) and nocodazole-treated (**C**,**D**) cells we transiently expressed PH-PLCδ–EGFP (green) and co-stained with Hoechst 33342 (blue). PH-PLCδ–EGFP is found at the plasma membrane and provides visual evidence of membrane deformation and tip indentation (A−D). In each case a cell was imaged before and during indentation over the course of 240 seconds. In the ZX projections taken along the dashed line (B,D) the triangular tip indentation is clearly visible after only 20 seconds of force application (20 nN for both). Importantly, the indentation does not noticeably increase over time. (**E**) The distance between the top and bottom of the cell at 0 seconds and the distance from the tip apex to the bottom of the cell after 240 seconds of an applied 20 nN force was plotted (white bars, untreated cells; grey bars, nocodazole-treated cells). Nocodazole treatment does not result in a significant increase in cell height ($P>0.84$). Moreover, the indentation in response to a 20 nN load after 240 seconds has no dependence on nocodazole treatment ($P>0.97$). All values are means ± s.e.m., $n=5$ for control and $n=3$ for nocodazole-treated cells Scale bars: 15 μm.

(supplementary material Fig. S4). Cells that were not treated with Y27632 did not show any such a response.

Strain dynamics In SFs

As noted above, the tracking technique employed thus far precludes the measurement of strain dynamics along the actin SFs. Actin SFs are thought to be tension-bearing structures that are able to contract and stretch through actomyosin-mediated processes. To investigate changes in tension along SFs we designed an experiment in which cells expressing actin–EGFP were photobleached to produce a regular pattern of low and high intensity regions, spaced every 5 μm, along the SFs in the cell (Kolsch et al., 2010). This resulted in intact SFs that were segmented and resembled dashed lines (Fig. 6). If SFs undergo stretching or contraction dynamics, this would cause changes in segment length allowing the local strain to be determined. To quantify the strain we measured a fluorescence intensity profile, $g(x)$, along SFs at each time point. For a particular fibre at a given time t, the intensity profile resembled a square wave as shown in

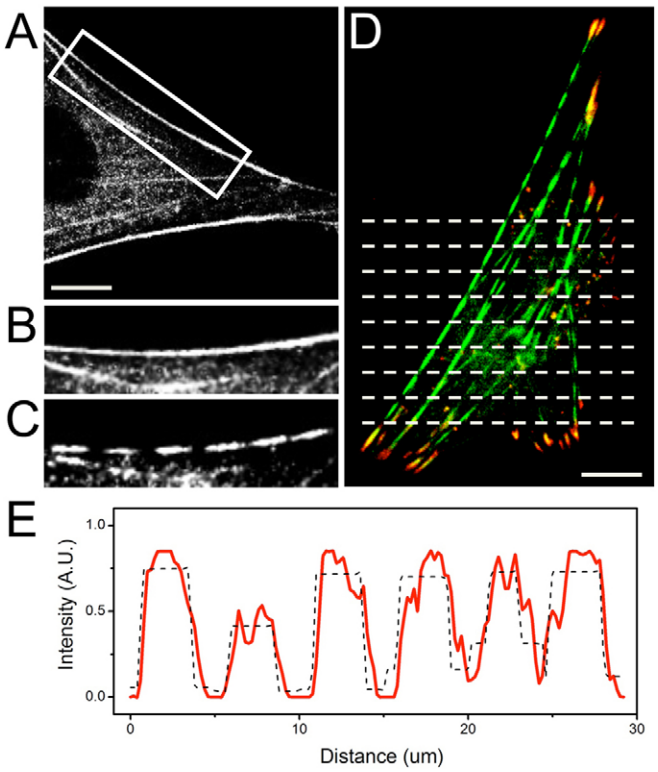

Fig. 6. Photobleaching and strain quantification of SFs. (**A**–**C**) Actin SFs were photobleached to produce a regular pattern of dark spots. The boxed region on A is shown at higher magnification before photobleaching in B and after photobleaching in C. (**D**) After a cell was chosen for measurement, linear regions of interest were laid out to produce a series of lines, as perpendicularly as possible to SF orientation and spaced every 5 μm. The cell here is expressing actin–EGFP and zyxin–mRFP and was photobleached along the dashed lines. The dashed lines are not shown at the top of the image in order to reveal the effect on intact SFs that have active EGFP in short segments along their length (note that the SF has not been physically altered). (**E**) In order to characterize changes in segment lengths we measured the fluorescence intensity profile along each SF (red line). We then developed a simple script (described in the text) that identified each peak in the profile and fitted a sum of approximate Heaviside functions to the data (black dashed line). The script was very successful at determining segment widths, however, in some cases, because of intensity noise, some peaks were not a good fit. In all cases the fits were checked by eye and poorly fitted peaks were removed from the analysis.

Fig. 6E. Using these data we created a script that automatically located and fitted each peak of the intensity profile to a sum of approximate Heaviside functions with the form:

$$g(x)=a\left[\frac{1}{1+\exp\left(-b\left(x-x_0+\frac{w_h}{2}\right)\right)}-\frac{1}{1+\exp\left(-b\left(x-x_0-\frac{w_h}{2}\right)\right)}\right]+\Delta$$

where x_0 is the peak position, w_h is the width of the peak, a is a normalization factor, b is a steepness factor, which we set to a satisfactory value of 10 and Δ is a shift. The positions x_l and widths w_l of the minima were then inferred from the values found for the peaks. The time evolution of the strain $\varepsilon(t)$ for a peak or minimum is given by:

$$\varepsilon(t)=\frac{w_t-w_0}{w_0}$$

where w_0 is the width of the peak or minimum at time zero. This approach was ~95% successful at correctly identifying features in the intensity profile. The fit often overshot or undershot the peak maximum but was extremely accurate at determining peak widths. In some cases, because of intensity noise, a width was overestimated but all fits were checked by eye and any misidentified peaks were removed from the analysis (Fig. 6E). Importantly, over the course of our measurement (240 seconds) we did not observe any fluorescence recovery after photobleaching (FRAP) (supplementary material Fig. S5). This is consistent with previous studies in which FRAP measurements revealed that F-actin in SFs have a relatively long recovery half time (~10 minutes and only 30% recovery after 240 seconds) and the majority of F-actin filaments in SFs are non-mobile (Campbell and Knight, 2007; Kreis et al., 1982; McGrath et al., 1998).

Measurements of strain dynamics were made on control cells and cells experiencing a 20 nN force, as described above. Colour maps of strain along SFs in a cell experiencing a 20 nN force are shown in Fig. 7. SFs in control and mechanically stimulated cells produced both positive (stretch) and negative (contraction) strains. The strain varied heterogeneously along SFs and throughout the cell. This phenomenon occurred regardless of force and varied considerably at each time interval, indicating that SFs undergo constant stretch and contraction dynamics along their lengths. To directly compare all the SFs measured in our study, we normalized the SF lengths and plotted the average strain measured as a function of fibre position and as a function of time (Fig. 7B,C; supplementary material Fig. S6). What becomes clear is that the strain fluctuated around a zero mean and the standard deviation (σ) of the strain along the fibre length was ~50% higher when the cell was experiencing a 20 nN stimulus (σ=0.22 at 20 nN; or σ=0.15 for control). Applied force appears to increase the number of negative strain events, indicating increased local contractions. Interestingly, the increase in σ occurred within the first 30 seconds of force application and remained constant over the 240 seconds examined (supplementary material Fig. S6). Strain fluctuations are likely to be mediated by myosin-II activity and are reflective of basal and force-induced upregulation of myosin activity.

Discussion

We have demonstrated the short-term response of actin SFs to locally applied forces over short time scales. Force was applied to living cells expressing actin–EGFP using an AFM cantilever positioned over the nucleus. Upon force application, two types of SF displacement were observed. The first was a small-scale deformation of SFs in close proximity to the nucleus. This took place in response to deformation of the nucleus (Maniotis et al., 1997). The second was highly localized and occurred far from the point of contact. In several cases this included the retraction of distant fibres at cell edges. SFs were generally located along the basal membrane of the cell, with the nucleus sitting above the plane of all fibres. As force was applied above the centre of the nucleus, we conclude that any movement of SFs was not a direct displacement caused by the indentation of the AFM tip, which is in agreement with PH-PLCδ–EGFP imaging (Fig. 5). However, in many cases, the nucleus was observed to expand or move in

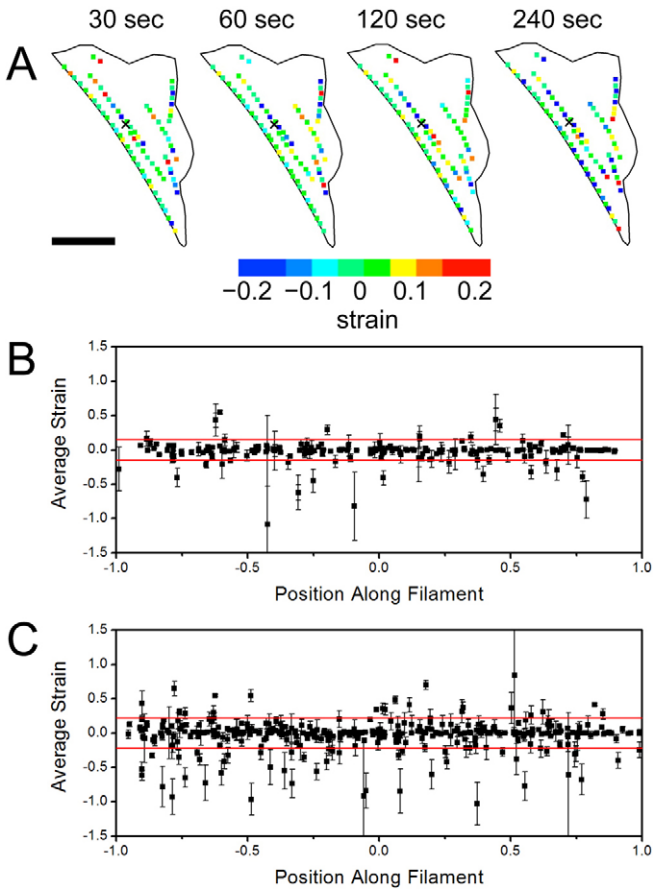

Fig. 7. Strain dynamics along SFs in control and mechanically stimulated cells. (**A**) A diagram of a cell experiencing an applied force of 20 nN. The strain along each SF is shown as a coloured spot according to magnitude (the contact point of the AFM cantilever is marked with a black 'x' and is over the centre of the nucleus). The strain magnitude and sign is heterogeneous along the length of any given filament and fluctuates in time, indicating rapid changes in stretch and contraction dynamics. Similar results were found for control cells (data not shown). Scale bar: 20 μm. (**B**,**C**) In order to compare SFs directly, we normalized their lengths between –1 and +1 and plotted the average strain observed as a function of position along the fibre after 240 seconds (similar plots were generated after 60, 120 and 180 seconds; see supplementary material Fig. S5). The measured strain tended to fluctuate around zero. However, the standard deviation (red lines) for control cells (B) is 0.15 and mechanically stimulated cells (C) is 0.22; i.e. ~50% higher in the stimulated cells. These strain fluctuations possibly reflect an increase in actomyosin activity in response to applied force. For the control, n=25 SFs in five cells. For the 20 nN stimulation, n=32 SFs in eight cells. Values are means ± s.e.m.

response to applied force. Slight deformation of SFs in the vicinity of the nucleus is likely due to this deformation.

To gauge experimental error in the quantification of SF displacement we imaged live cells with no applied force and after fixing cells with paraformaldehyde. In the latter case, SFs should not move at all and any displacement that is observed will be due to microscope drift and/or tracking errors. As can be seen in Fig. 2A, there is a small amount of drift in the tracking but it is well below the measured response of cells exposed to 0–20 nN of force. Extending our analysis further, we calculated the difference in percentage of all tracking points having a non-zero displacement at every time point in all cells being exposed to force and all cells that were fixed (supplementary material Fig. S7). After ~120 seconds of force application, the percentage of moving points reached a plateau at each applied force. When compared with the data for the average displacement as a function of time we can clearly see that although the average displacement continues to increase after ~120 seconds for all forces, the number of points moving along a SF has become constant. This suggests that the number of SFs undergoing some sort of movement steeply increases within the first 120 seconds of force application and after this point no other filaments begin to move. Therefore, the direct response of SFs to force is greatest within 20–120 seconds of contact with the AFM tip. At later times, SF remodelling is no longer a response to a force-induced deformation but due to other processes such as FA movement (Trache and Lim, 2009). Importantly, we found absolutely no evidence that the magnitude of local SF displacement had any dependence on the distance between the SF position and the AFM tip.

To clearly characterize the remodelling of SF-associated FA sites, cells transiently expressing actin–EGFP and zyxin–mRFP were examined. Zyxin has been proposed as a 'tension sensing' protein that is recruited to FA complexes as they form along actin SFs and anchors cells to the substrate (Colombelli et al., 2009; Lele et al., 2006). Moreover, there is a strong correlation between zyxin localization and F-actin anchor and stress points (Rottner et al., 2001). As can be seen in supplementary material Fig. S2, the movement of SFs that retract following force application is correlated with the movement of zyxin-rich FA sites. This suggests that the mechanical stimulus results in FA remodelling at later time points, which causes SF movement far from the point of contact. Moreover, the zyxin–mRFP signal on moving SFs was not observed to diminish over time, which suggests the localized tension near the FA site remains constant during displacement.

Movement of SFs far from the point of contact (~30–50 μm) following force application and the lack of any observed large scale isotropic deformation suggest that other components of the cytoarchitecture are involved in transmission of the mechanical stimulus. To investigate the contribution of MTs, cells were treated with nocodazole. Cells chosen for study were generally smaller and remained attached with intact SFs. The cortical Young's modulus of the treated cells was determined to be almost half that of cells without drug treatment (~4 kPa versus ~7 kPa, respectively). Cells treated with nocodazole were then submitted to a 20 nN force. SFs were tracked as before and the average displacement of all data points was calculated over time. In Fig. 2B, we observed that nocodazole treatment is sufficient to reduce SF displacement to the same level as in control cells (with or without nocodazole), which can be attributed to the normal dynamics of actin SFs. What is clear is that although the cells have a lower cortical elasticity, no significant displacement of the SF network was observed over that of controls and no isotropic deformation took place. As the MT network has been eliminated in these cells, the results suggest that the crosstalk and interplay between MTs and SFs plays an important role in force transmission through the cell (Even-Ram et al., 2007; Pelling et al., 2009). In order to confirm that the change in SF deformation was not due to nocodazole-induced changes in cell height or indentation depth of the AFM cantilever we created cells transiently expressing PH-PLCδ–EGFP to visualize the cell

membrane. As shown in Fig. 5, there was no significant difference in initial height or indentation depth at 20 nN force in control and nocodazole-treated cells. Additionally, an AFM tip applying a 20 nN force did not penetrate all the way through the cells in either condition, even after 4 minutes of force application. There was typically a distance of ~6–7 μm between the tip apex and the bottom of the cell. Therefore, there was never any direct contact between the AFM tip and the SFs (Figs 1, 5). The results also demonstrate the deformability of the nucleus. The mechanical and physical properties of the nucleus are known to influence the biology of the cell (Dahl et al., 2006; Pajerowski et al., 2007; Wang et al., 2009), and mechanical forces can be transmitted to the nucleus through the cytoskeleton (Maniotis et al., 1997; Wang et al., 2009). However, as we have shown here, nanoscale forces applied directly to the nucleus not only result in chromatin deformation but also much wider whole cell cytoarchitectural remodelling. Although we suspect that some displacement of SFs close to the point of contact is due directly to nuclear deformation, it is clear that SF movements occurring far from the point of contact are due to localized transmission of the applied nanomechancial force (Hu et al., 2004; Silberberg et al., 2008).

The rho pathway is integral to the formation of actin SFs and their contraction during cell expansion and motility (Fukata et al., 2001). Inhibition of ROCK with Y27632 eliminates the formation of intact F-actin filaments. Treatment with Y27632 results in a rounded cell morphology and a cortical Young's modulus of ~1 kPa, seven times smaller than that of native cells. Although there are no intact SFs, there remains a visible response of the cell to the application of 20 nN of force. In this case, the diameter of the rounded cell body was measured as a function of time. A distinct isotropic bulging around the nucleus (supplementary material Fig. S4) was apparent immediately following force application. After removal of the force the cell then returned to its initial dimensions. Interestingly, retraction of cell edges in response to force was not observed. This implies that cell edge retraction is not possible without SFs, and is consistent with inhibition of ROCK, as there is no contraction mechanism available.

Creating a series of photobleached regions across SFs (Kolsch et al., 2010) allowed us to determine the strain dynamics occurring along cellular SFs in response to mechanical stimulation. Strain dynamics along SFs and throughout the cell were highly heterogeneous and time variant. There is also no clear dependence of strain magnitude (and sign) on the position along the SFs where the measurements were taken. This is generally consistent with a previous study (Peterson et al., 2004) in which calyculin A induced a non-uniform contraction along SFs. However, treatment with calyculin A is a drastic approach to stimulate a contraction and resulted in the observation that SFs contract at their ends and stretch more in the middle of the fibre. By contrast, we have been able to characterize basal fluctuations in strain in unperturbed and mechanically stimulated cells. From our measurements we characterized the fluctuations in strain along SFs as $\sigma=0.22$ at 20 nN and $\sigma=0.15$ for control cells. It is tempting to obtain an estimate for the magnitude of force acting on the filament to produce such a strain fluctuation. Consider a case where we assume an outside force is acting on a section of SF and causes a local positive strain (stretch) of 0.15 or 0.22. The Young's modulus and diameter of SFs have been estimated to be ~300 kPa and ~250 nm, respectively (Deguchi et al., 2005). Assuming a simple stress–strain relationship we can estimate the force producing the strain fluctuations to be ~2–3 nN. Conversely, if myosin contractions within the fibre were driving the observed strain fluctuations this would imply the ability to generate 2–3 nN of force. This is not completely out of the range of possibility, considering that a single myosin fibre typically generates ~2 pN of force (Veigel et al., 2003) and the contractile force of SFs have been measured in the 0.5–4 nN range (Deguchi et al., 2005; Thoresen et al., 2011). However, the Young's modulus we have used here, and in previous estimates of contractile force, were determined on reconstituted or isolated SFs (Deguchi et al., 2005; Thoresen et al., 2011). The effective Young's modulus of SFs in a living cell could be much higher because of crosslinking with the rest of the cytoarchitecture (Even-Ram et al., 2007), and has been estimated to be as high as 1 GPa (Kojima et al., 1994). If this were the case, external or internal forces would have to be tens, if not hundreds, of nanonewtons to produce such strains. Therefore, the role of crosslinking on the effective mechanical properties of SFs in the cell cannot be ignored.

We speculate that the strain dynamics observed here might in fact be the result of myosin-driven movement of the short F-actin filaments in SFs (Fig. 8). Ventral SFs (Pellegrin and Mellor, 2007), such as those observed in this study, are composed of 1–2 μm F-actin filaments, ~0.6 μm long myosin-II thick filaments, α-actinin and filamin (Pellegrin and Mellor, 2007). In response to a mechanical stimulus, Ca^{2+} release occurs (Formigli et al., 2007b), which induces a calmodulin-mediated activation of myosin light chain kinase (MLCK), ultimately resulting in increased SF formation and myosin contraction (Fukata et al., 2001). In our experiment we photobleached SFs to create a regular pattern of light-emitting and photobleached regions. Let us assume that for a given light-emitting region of the SF, myosin contraction causes F-actin–GFP filaments to move and produce an apparent negative strain (Fig. 8). This will cause an apparent positive strain in the neighbouring photobleached region. The converse phenomenon might also occur, in which contraction takes place in a photobleached region. Moreover, because SFs are highly crosslinked with the cytoskeleton and focal adhesion sites (Even-Ram et al., 2007), short SF regions with a variable number of crosslinks to the cytoarchitecture exist. This will cause localized variations in the effective Young's modulus in the nanometre to micometre length scale and result in regions of the SF that are prevented from undergoing deformation or strain, and others that can easily do so. This picture is consistent with our experimental data: we observed a heterogeneous distribution of strain along SFs and localized force-induced lateral deformations. Importantly, applied force appears to mechanically stimulate actomyosin activity through activation of MLCK, causing an increase in strain fluctuations by ~50% over baseline levels within 30 seconds of applied force (Fukata et al., 2001).

In summary, our results demonstrate distinct responses of actin SFs in fibroblast cells to nanoscale forces applied above the nucleus. Importantly, these responses take place well before, and probably govern, the long-term structural reorganization of the SF cytoskeleton in response to force (Trache and Lim, 2009). They consist of a short-term response (20–60 seconds) in which SFs deform as a direct result of an applied force, and a long-term response (60–240 seconds) in which applied forces initiate FA remodelling and movement of SFs far from the point of contact. Moreover, SF deformation does not occur in an isotropic fashion,

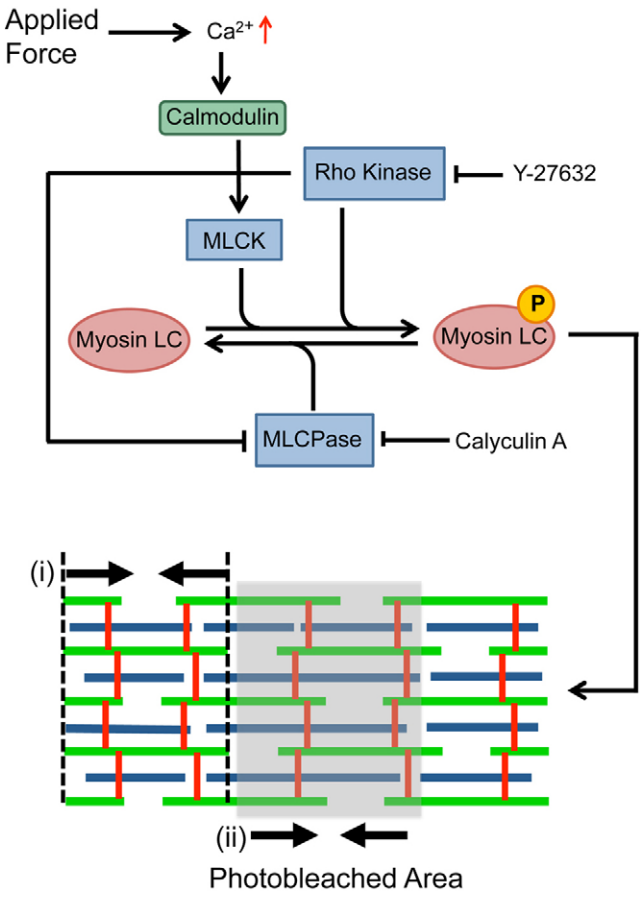

Fig. 8. Possible mechanotransduction pathway to account for the observed strain dynamics. The rho pathway (top panel) has been well characterized and is involved directly in the regulation of actomyosin contractility. We suggest that an externally applied force results in an increase in Ca^{2+} ions, which induce a calmodulin-dependent activation of myosin light chain kinase (MLCK). This kinase, as well as ROCK (rho kinase), phosphorylates the light chain of myosin II (Myosin LC) activating it and causing increased contraction and SF formation. This would have a similar effect to treatment with calyculin A, which is an inhibitor of myosin light chain phosphatase (MLCPase); this effectively blocks the inactivation of myosin II, constitutively activating contraction throughout the cell. These cascades will probably lead to contraction dynamics within the unbleached (i) and bleached (ii) segments of SFs (schematic in lower panel; green, F-actin; blue, myosin thick filaments; red, α-actinin). Owing to the highly cross-linked nature of SFs with the cytoskeleton, contraction in one segment will not necessarily lead to expansion in the adjacent segment or vice versa.

but in localized regions. In some cases a few SFs retract but this does not result in a retraction of the cell. The cell remains firmly attached to the substrate by intact FA sites, even on retracting F-actin filaments. The most immediate response of a cell to a mechanical stimulus is complex structural deformation that requires the integration of several elements of the cytoskeleton. Cells lacking an intact MT network do not show any appreciable SF displacements. We suggest that a force-dependent signal is transmitted through the MT network to SFs and some FA sites, resulting in deformation and retraction. In this study, we have also characterized the apparent strain dynamics that take place along SFs with and without a nanomechanical stimulus. We show that these strain dynamics are heterogeneous along the SF and suggest that strain dynamics are caused by the internal movement of F-actin filaments by myosin. Importantly, the activity of localized myosin-mediated contraction increases in response to a mechanical stimulus by as much as 50%. This suggests that we have directly visualized the contraction of actomyosin in vitro in non-sarcomeric actin SFs. These results are intriguing and future work will focus on developing similar assays with increased temporal and spatial resolution to investigate the origin of heterogeneous strain dynamics and their spatial relationship with crosslinks between SFs and the rest of the cytoskeleton.

Mechanical stimuli are crucial factors that are involved in regulating the biology of the cell, but the short-term structural response of a cell to mechanical deformation remains relatively poorly understood. In this study, we have shown that fibroblast cells possess several clear force-dependent responses to mechanical stimulation. Force application does not result in an isotropic deformation of the SF cytoskeleton, but rather, results in a complex and localized response that is dependent on an intact MT network. Furthermore, force-dependent increased actomyosin activity results in non-uniform contraction and stretch dynamics taking place along the SFs. Direct visualization of force-propagation in this study has revealed several crucial and complex phenomena that require the integration of the entire cytoskeleton and ultimately govern the long-term downstream response of a cell to mechanical stimuli.

Materials and Methods

Cell culture

NIH3T3 mouse fibroblast cells were cultured in DMEM, supplemented with 10% heat-inactivated FBS, 100 IU/ml penicillin and 100 µg/ml streptomycin (Hyclone). Cells were cultured at 37℃ in 5% CO_2 on 100-mm tissue culture dishes (Corning) or seeded on 35-mm glass-bottomed dishes (Mat Tek) for experiments.

Plasmids and transfections

Zyxin–mRFP plasmid was a kind gift from Anna Huttenlocher (Bhatt et al., 2002). Plasmids for actin–EGFP and the PH domain of PLCδ conjugated to EGFP (PH-PLCδ–EGFP) have been described previously (Hemsley et al., 2011; Pelling et al., 2009). Transfections were performed using Lipofectamine 2000 (Invitrogen) and 1 µg DNA at a ratio of 4:1 according to manufacturer's specifications. Experiments were performed 2 days after transfection.

Drug treatments

Cells were treated with nocodazole (Sigma) dissolved in DMSO (Fisher Scientific) for approximately 15 minutes (Pelling et al., 2009) at a final concentration of 10 µM, and were maintained at 37℃ while on the microscope stage. Cells were treated with Y27632 (Sigma) dissolved in water at a final concentration of 10 µM for 30 minutes in an incubator at 37℃ and 5% CO_2 before experiments.

Immunofluorescence staining

Briefly, cells were fixed with 3.5% paraformaldehyde and permeabilized using Triton X-100 at 37℃. Cells were stained for actin using Phalloidin–Alexa-Fluor-546 (Invitrogen). MTs were stained with a mouse monoclonal anti-α-tubulin (Abcam) primary antibody followed by an Alexa Fluor 488 rabbit anti-mouse immunoglobin (Invitrogen) secondary antibody. DNA was stained using DAPI (Invitrogen). A full protocol was published previously (Pelling et al., 2009).

Simultaneous atomic force microscopy and confocal microscopy

All images of living and fixed cells were acquired on a Nikon TiE A1-R (Nikon) high-speed resonant laser scanning confocal microscope (LSCM) with a 60×, 1.2 NA water immersion lens. An AFM (NanoWizard II, JPK Instruments) was integrated with the LSCM for simultaneous measurements. AFM–LSCM experiments were performed as follows: after an appropriate cell that was transiently expressing fluorescently tagged proteins was located, four-dimensional LSCM imaging was commenced. Image volumes were acquired every 20 seconds for 5 minutes. After 60 seconds of imaging with no applied force the AFM tip was brought into contact with the cell (over the centre of the nucleus) and a constant force was applied [0 (control), 1, 5, 10 or 20 nN]. In all AFM–LSCM measurements the nucleus was stained with Hoechst 33342 (Invitrogen) according to manufacturer's protocols to identify live cells. MSCT-AUHW

gold-coated SiN_4 cantilevers were used in all experiments (Veeco). Spring constants ($k=0.07\pm0.03$ N/m) were determined by the thermal fluctuation method before all measurements (Hutter and Bechhoefer, 1993; Lévy and Maaloum, 2002). The Young's modulus of the cortex of the cells was determined by analyzing force curves with the Hertz model for 200 nm indentations (Matzke et al., 2001).

In some experiments, we employed photobleaching to create fiduciary markers along actin SFs. Cells transiently expressing actin–EGFP had a series of lines photobleached into the SFs before experimentation (Kolsch et al., 2010). A series of regions of interest (ROI) were created from 1.5 μm wide parallel lines spaced every 5 μm. The ROIs were oriented such that the maximal number of SFs was crossed perpendicularly. Photobleaching was performed in the ROIs with a 488 nm laser set at 100% power for 10 bleach iterations. AFM–LSCM experiments were then performed as above.

Image and statistical analysis

Images were analyzed with ImageJ (http://rsb.info.nih.gov/ij/) and the MTrackJ plugin (http://www.imagescience.org/meijering/software/mtrackj/). Images of fixed and stained cells are maximum intensity *Z*-projections of all slices and were adjusted to maximize the fluorophore signal; no other enhancements were applied. All images of live actin–EGFP transfected cells are maximum intensity *Z*-projections of the confocal planes that contained SFs (~2–5 μm thick). Points along SFs [separated by ~5 μm, which is less than the persistence length of F-actin (Arai et al., 1999; Brangwynne et al., 2007; van Mameren et al., 2009)] were tracked over the course of the experiment. SF displacement was measured at these points as a function of time and averaged over all points for all SFs. Kymographs (plots of intensity versus time) were created using ImageJ to re-slice the image along a line drawn perpendicular to SFs or focal adhesion sites. Kymographs can be used to clearly visualize the movement of a particular image feature as a function of time. Images of photobleached actin–EGFP SFs were analyzed by measuring an intensity profiles along an SF containing the bleached pattern. A script (described in the Results) was employed to semi-automatically determine the width of each of the bleached regions, allowing for the determination of strain dynamics along SFs over time. All values quoted in this study are means ± s.e.m.; *n*-values and *P*-values (determined with a Student's *t*-test, $\alpha=0.05$) are given in the figure legends.

Funding

L.G. was supported by graduate fellowships from the Natural Sciences and Engineering Research Council (Canada) and the Ontario Graduate Scholarships program; M.B. was supported by a Natural Sciences and Engineering Research Council (Canada) Discovery Grant to Béla Joós, University of Ottawa [grant number RGPIN/008671-2006]. This work was supported by a Natural Sciences and Engineering Research Council Discovery Grant [grant number RGPIN/355535-2009 to A.E.P.] and Discovery Accelerator Supplement [grant number RGPAS/380321-2009 to A.E.P.]; the Canada Research Chairs program [grant number 950-206182 to A.E.P.]; and a Province of Ontario Early Researcher Award [grant number ER09-06-158 to A.E.P.].

Supplementary material available online at
http://jcs.biologists.org/lookup/suppl/doi:10.1242/jcs.088302/-/DC1

References

Albrecht-Buehler, G. (1987). Role of cortical tension in fibroblast shape and movement. *Cell Motil. Cytoskeleton* **7**, 54-67.

Arai, Y., Yasuda, R., Akashi, K., Harada, Y., Miyata, H., Kinosita, K., Jr and Itoh, H. (1999). Tying a molecular knot with optical tweezers. *Nature* **399**, 446-448.

Bhatt, A., Kaverina, I., Otey, C. and Huttenlocher, A. (2002). Regulation of focal complex composition and disassembly by the calcium-dependent protease calpain. *J. Cell Sci.* **115**, 3415-3425.

Binnig, G., Quate, C. F. and Gerber, C. (1986). Atomic force microscope. *Phys. Rev. Lett.* **56**, 930-933.

Brangwynne, C. P., Koenderink, G. H., Barry, E., Dogic, Z., MacKintosh, F. C. and Weitz, D. A. (2007). Bending dynamics of fluctuating biopolymers probed by automated high-resolution filament tracking. *Biophys. J.* **93**, 346-359.

Burridge, K., Fath, K., Kelly, T., Nuckolls, G. and Turner, C. (1988). Focal adhesions: transmembrane junctions between the extracellular matrix and the cytoskeleton. *Annu. Rev. Cell. Biol.* **4**, 487-525.

Campbell, J. J. and Knight, M. M. (2007). An improved confocal FRAP technique for the measurement of long-term actin dynamics in individual stress fibers. *Microsc. Res. Tech.* **70**, 1034-1040.

Charras, G. T. and Horton, M. A. (2002a). Determination of cellular strains by combined atomic force microscopy and finite element modeling. *Biophys. J.* **83**, 858-879.

Charras, G. T. and Horton, M. A. (2002b). Single cell mechanotransduction and its modulation analyzed by atomic force microscope indentation. *Biophys. J.* **82**, 2970-2981.

Charras, G. T., Williams, B. A., Sims, S. M. and Horton, M. A. (2004). Estimating the sensitivity of mechanosensitive ion channels to membrane strain and tension. *Biophys. J.* **87**, 2870-2884.

Chiquet, M., Tunc-Civelek, V. and Sarasa-Renedo, A. (2007). Gene regulation by mechanotransduction in fibroblasts. *Appl. Physiol. Nutr. Metab.* **32**, 967-973.

Chowdhury, F., Na, S., Li, D., Poh, Y. C., Tanaka, T. S., Wang, F. and Wang, N. (2010). Material properties of the cell dictate stress-induced spreading and differentiation in embryonic stem cells. *Nat. Mater.* **9**, 82-88.

Colombelli, J., Besser, A., Kress, H., Reynaud, E. G., Girard, P., Caussinus, E., Haselmann, U., Small, J. V., Schwarz, U. S. and Stelzer, E. H. (2009). Mechanosensing in actin stress fibers revealed by a close correlation between force and protein localization. *J. Cell Sci.* **122**, 1665-1679.

Costa, K. D. (2006). Imaging and probing cell mechanical properties with the atomic force microscope. *Methods Mol. Biol.* **319**, 331-361.

Costa, K. D., Sim, A. J. and Yin, F. C. (2006). Non-Hertzian approach to analyzing mechanical properties of endothelial cells probed by atomic force microscopy. *J. Biomech. Eng.* **128**, 176-184.

Czajkowsky, D. M., Iwamoto, H. and Shao, Z. (2000). Atomic force microscopy in structural biology: from the subcellular to the submolecular. *J. Electron. Microsc.* **49**, 395-406.

Dahl, K. N., Scaffidi, P., Islam, M. F., Yodh, A. G., Wilson, K. L. and Misteli, T. (2006). Distinct structural and mechanical properties of the nuclear lamina in Hutchinson-Gilford progeria syndrome. *Proc. Natl. Acad. Sci. USA* **103**, 10271-10276.

Deguchi, S., Ohashi, T. and Sato, M. (2005). Evaluation of tension in actin bundle of endothelial cells based on preexisting strain and tensile properties measurements. *Mol. Cell. Biomech.* **2**, 125-133.

Engler, A. J., Sen, S., Sweeney, H. L. and Discher, D. E. (2006). Matrix elasticity directs stem cell lineage specification. *Cell* **126**, 677-689.

Even-Ram, S., Doyle, A. D., Conti, M. A., Matsumoto, K., Adelstein, R. S. and Yamada, K. M. (2007). Myosin IIA regulates cell motility and actomyosin-microtubule crosstalk. *Nat. Cell Biol.* **9**, 299-309.

Fletcher, D. A. and Mullins, R. D. (2009). Cell mechanics and the cytoskeleton. *Nature* **463**, 485-492.

Formigli, L., Meacci, E., Sassoli, C., Squecco, R., Nosi, D., Chellini, F., Naro, F., Francini, F. and Zecchi-Orlandini, S. (2007a). Cytoskeleton/stretch-activated ion channel interaction regulates myogenic differentiation of skeletal myoblasts. *J. Cell. Physiol.* **211**, 296-306.

Formigli, L., Meacci, E., Zecchi-Orlandini, S. and Orlandini, G. E. (2007b). Cytoskeletal reorganization in skeletal muscle differentiation: from cell morphology to gene expression. *Eur. J. Histochem.* **51 Suppl. 1**, 21-28.

Fukata, Y., Amano, M. and Kaibuchi, K. (2001). Rho-Rho-kinase pathway in smooth muscle contraction and cytoskeletal reorganization of non-muscle cells. *Trends Pharmacol. Sci.* **22**, 32-39.

Haupt, B. J., Pelling, A. E. and Horton, M. A. (2006). Integrated confocal and scanning probe microscopy for biomedical research. *Scientific World Journal* **6**, 1609-1618.

Hayakawa, K., Tatsumi, H. and Sokabe, M. (2008). Actin stress fibers transmit and focus force to activate mechanosensitive channels. *J. Cell Sci.* **121**, 496-503.

Heidemann, S. R., Kaech, S., Buxbaum, R. E. and Matus, A. (1999). Direct observations of the mechanical behaviors of the cytoskeleton in living fibroblasts. *J. Cell Biol.* **145**, 109-122.

Hemsley, A. L., Hernandez, D., Mason, C., Pelling, A. E. and Veraitch, F. S. (2011). Precisely delivered nanomechanical forces induce blebbing in undifferentiated mouse embryonic stem cells. *Cell Health Cytoskelet.* **3**, 23-34.

Henderson, E., Haydon, P. G. and Sakaguchi, D. S. (1992). Actin filament dynamics in living glial cells imaged by atomic force microscopy. *Science* **257**, 1944-1946.

Hogan, C., Dupre-Crochet, S., Norman, M., Kajita, M., Zimmermann, C., Pelling, A. E., Piddini, E., Baena-Lopez, L. A., Vincent, J. P., Itoh, Y. et al. (2009). Characterization of the interface between normal and transformed epithelial cells. *Nat. Cell Biol.* **11**, 460-467.

Hoh, J. H. and Schoenenberger, C. A. (1994). Surface morphology and mechanical properties of MDCK monolayers by atomic force microscopy. *J. Cell Sci.* **107**, 1105-1114.

Hu, S., Eberhard, L., Chen, J., Love, J. C., Butler, J. P., Fredberg, J. J., Whitesides, G. M. and Wang, N. (2004). Mechanical anisotropy of adherent cells probed by a three-dimensional magnetic twisting device. *Am. J. Physiol. Cell Physiol.* **287**, C1184-C1191.

Hutter, J. L. and Bechhoefer, J. (1993). Calibration of atomic force microscope tips. *Rev. Sci. Instrum.* **64**, 1868-1873.

Jaalouk, D. E. and Lammerding, J. (2009). Mechanotransduction gone awry. *Nat. Rev. Mol. Cell Biol.* **10**, 63-73.

Ko, K. S. and McCulloch, C. A. (2000). Partners in protection: interdependence of cytoskeleton and plasma membrane in adaptations to applied forces. *J. Membr. Biol.* **174**, 85-95.

Kojima, H., Ishijima, A. and Yanagida, T. (1994). Direct measurement of stiffness of single actin filaments with and without tropomyosin by in vitro nanomanipulation. *Proc. Natl. Acad. Sci. USA* **91**, 12962-12966.

Kolsch, A., Windoffer, R., Wurflinger, T., Aach, T. and Leube, R. E. (2010). The keratin-filament cycle of assembly and disassembly. *J. Cell Sci.* **123**, 2266-2272.

Kreis, T. E., Geiger, B. and Schlessinger, J. (1982). Mobility of microinjected rhodamine actin within living chicken gizzard cells determined by fluorescence photobleaching recovery. *Cell* **29**, 835-845.
Kumar, S., Maxwell, I. Z., Heisterkamp, A., Polte, T. R., Lele, T. P., Salanga, M., Mazur, E. and Ingber, D. E. (2006). Viscoelastic retraction of single living stress fibers and its impact on cell shape, cytoskeletal organization, and extracellular matrix mechanics. *Biophys. J.* **90**, 3762-3773.
Kunda, P., Pelling, A. E., Liu, T. and Baum, B. (2008). Moesin controls cortical rigidity, cell rounding, and spindle morphogenesis during mitosis. *Curr. Biol.* **18**, 91-101.
Lehenkari, P. P., Charras, G. T., Nykanen, A. and Horton, M. A. (2000). Adapting atomic force microscopy for cell biology. *Ultramicroscopy* **82**, 289-295.
Lele, T. P., Pendse, J., Kumar, S., Salanga, M., Karavitis, J. and Ingber, D. E. (2006). Mechanical forces alter zyxin unbinding kinetics within focal adhesions of living cells. *J. Cell. Physiol.* **207**, 187-194.
Lévy, R. and Maaloum, M. (2002). Measuring the spring constant of atomic force microscope cantilevers: thermal fluctuations and other methods. *Nanotechnology* **13**, 33-37.
Lopez, J. I., Mouw, J. K. and Weaver, V. M. (2008). Biomechanical regulation of cell orientation and fate. *Oncogene* **27**, 6981-6993.
Maloney, J. M., Nikova, D., Lautenschläger, F., Clarke, E., Langer, R., Guck, J. and Van Vliet, K. J. (2010). Mesenchymal stem cell mechanics from the attached to the suspended state. *J. Biophys.* **99**, 2479-2487.
Maniotis, A. J., Chen, C. S. and Ingber, D. E. (1997). Demonstration of mechanical connections between integrins, cytoskeletal filaments, and nucleoplasm that stabilize nuclear structure. *Proc. Natl. Acad. Sci. USA* **94**, 849-854.
Matzke, R., Jacobson, K. and Radmacher, M. (2001). Direct, high-resolution measurement of furrow stiffening during division of adherent cells. *Nat. Cell Biol.* **3**, 607-610.
McGrath, J. L., Tardy, Y., Dewey, C. F., Jr, Meister, J. J. and Hartwig, J. H. (1998). Simultaneous measurements of actin filament turnover, filament fraction, and monomer diffusion in endothelial cells. *Biophys. J.* **75**, 2070-2078.
Mierke, C. T. (2009). The role of vinculin in the regulation of the mechanical properties of cells. *Cell Biochem. Biophys.* **53**, 115-126.
Mott, R. E. and Helmke, B. P. (2007). Mapping the dynamics of shear stress-induced structural changes in endothelial cells. *Am. J. Physiol. Cell Physiol.* **293**, C1616-C1626.
Narumiya, S., Ishizaki, T. and Uehata, M. (2000). Use and properties of ROCK-specific inhibitor Y-27632. *Methods Enzymol.* **325**, 273-284.
Nix, D. A., Fradelizi, J., Bockholt, S., Menichi, B., Louvard, D., Friederich, E. and Beckerle, M. C. (2001). Targeting of zyxin to sites of actin membrane interaction and to the nucleus. *J. Biol. Chem.* **276**, 34759-34767.
Pajerowski, J. D., Dahl, K. N., Zhong, F. L., Sammak, P. J. and Discher, D. E. (2007). Physical plasticity of the nucleus in stem cell differentiation. *Proc. Natl. Acad. Sci. USA* **104**, 15619-15624.
Pellegrin, S. and Mellor, H. (2007). Actin stress fibres. *J. Cell Sci.* **120**, 3491-3499.
Pelling, A. E., Dawson, D. W., Carreon, D. M., Christiansen, J. J., Shen, R. R., Teitell, M. A. and Gimzewski, J. K. (2007a). Distinct contributions of microtubule subtypes to cell membrane shape and stability. *Nanomedicine* **3**, 43-52.
Pelling, A. E., Veraitch, F. S., Pui-Kei Chu, C., Nicholls, B. M., Hemsley, A. L., Mason, C. and Horton, M. A. (2007b). Mapping correlated membrane pulsations and fluctuations in human cells. *J. Mol. Recognit.* **20**, 467-475.
Pelling, A. E., Veraitch, F. S., Chu, C. P., Mason, C. and Horton, M. A. (2009). Mechanical dynamics of single cells during early apoptosis. *Cell Motil. Cytoskeleton* **66**, 409-422.
Peterson, L. J., Rajfur, Z., Maddox, A. S., Freel, C. D., Chen, Y., Edlund, M., Otey, C. and Burridge, K. (2004). Simultaneous stretching and contraction of stress fibers in vivo. *Mol. Biol. Cell* **15**, 3497-3508.
Radmacher, M. (2007). Studying the mechanics of cellular processes by atomic force microscopy. *Methods Cell Biol.* **83**, 347-372.
Radmacher, M., Tillamnn, R. W., Fritz, M. and Gaub, H. E. (1992). From molecules to cells: imaging soft samples with the atomic force microscope. *Science* **257**, 1900-1905.
Rotsch, C. and Radmacher, M. (2000). Drug-induced changes of cytoskeletal structure and mechanics in fibroblasts: an atomic force microscopy study. *Biophys. J.* **78**, 520-535.
Rottner, K., Krause, M., Gimona, M., Small, J. V. and Wehland, J. (2001). Zyxin is not colocalized with vasodilator-stimulated phosphoprotein (VASP) at lamellipodial tips and exhibits different dynamics to vinculin, paxillin, and VASP in focal adhesions. *Mol. Biol. Cell* **12**, 3103-3113.
Sato, M., Levesque, M. J. and Nerem, R. M. (1987). Micropipette aspiration of cultured bovine aortic endothelial cells exposed to shear stress. *Arterioscler. Thromb. Vasc. Biol.* **7**, 276-286.
Silberberg, Y. R., Pelling, A. E., Yakubov, G. E., Crum, W. R., Hawkes, D. J. and Horton, M. A. (2008). Mitochondrial displacements in response to nanomechanical forces. *J. Mol. Recognit.* **21**, 30-36.
Thoresen, T., Lenz, M. and Gardel, M. L. (2011). Reconstitution of contractile actomyosin bundles. *Biophys. J.* **100**, 2698-2705.
Trache, A. and Lim, S. M. (2009). Integrated microscopy for real-time imaging of mechanotransduction studies in live cells. *J. Biomed. Opt.* **14**, 034024.
Ueki, Y., Uda, Y., Sakamoto, N. and Sato, M. (2010). Measurements of strain on single stress fibers in living endothelial cells induced by fluid shear stress. *Biochem. Biophys. Res. Commun.* **395**, 441-446.
van Mameren, J., Vermeulen, K. C., Gittes, F. and Schmidt, C. F. (2009). Leveraging single protein polymers to measure flexural rigidity. *J. Phys. Chem. B* **113**, 3837-3844.
Veigel, C., Molloy, J. E., Schmitz, S. and Kendrick-Jones, J. (2003). Load-dependent kinetics of force production by smooth muscle myosin measured with optical tweezers. *Nat. Cell Biol.* **5**, 980-986.
Wang, N., Tytell, J. D. and Ingber, D. E. (2009). Mechanotransduction at a distance: mechanically coupling the extracellular matrix with the nucleus. *Nat. Rev. Mol. Cell Biol.* **10**, 75-82.
Weisberg, E., Sattler, M., Ewaniuk, D. S. and Salgia, R. (1997). Role of focal adhesion proteins in signal transduction and oncogenesis. *Crit. Rev. Oncog.* **8**, 343-358.

Journal of Cell Science